

1 **Role of OH variability in the stalling of the global atmospheric CH₄ growth**
2 **rate from 1999 to 2006**

3 **J. McNorton^{1,2}, M. P. Chipperfield^{1,2}, M. Gloor³, C. Wilson^{1,2}, W. Feng^{1,4},**
4 **G. D. Hayman⁵, M. Rigby⁶, P. B. Krummel⁷, S. O'Doherty⁶, R. G. Prinn⁸, R. F. Weiss⁹,**
5 **D. Young⁶, E. Dlugokencky¹⁰, and S. A. Montzka¹⁰**

6 1. School of Earth and Environment, University of Leeds, Leeds, LS2 9JT, UK.

7 2. National Centre for Earth Observation, University of Leeds, LS2 9JT, UK.

8 3. School of Geography, University of Leeds, Leeds, LS2 9JT, UK.

9 4. National Centre for Atmospheric Science, University of Leeds, LS2 9JT, UK.

10 5. Centre for Ecology and Hydrology, Wallingford, UK.

11 6. School of Chemistry, University of Bristol, Bristol, BS8 1TS, UK.

12 7. CSIRO Oceans and Atmosphere Flagship, Aspendale, Victoria, Australia.

13 8. Center for Global Change Science, Massachusetts Institute of Technology, Cambridge,
14 MA 02139, USA.

15 9. Scripps Institution of Oceanography, University of California, San Diego, CA 92093, USA.

16 10. National Oceanic and Atmospheric Administration, Boulder, USA.

17 **Abstract**

18 The growth in atmospheric methane (CH₄) concentrations over the past two decades has shown
19 large variability on a timescale of several years. Prior to 1999 the globally averaged CH₄
20 concentration was increasing at a rate of 6.0 ppb/yr, but during a stagnation period from 1999
21 to 2006 this growth rate slowed to 0.6 ppb/yr. From 2007 to 2009 the growth rate again
22 increased to 4.9 ppb/yr. These changes in growth rate are usually ascribed to variations in CH₄
23 emissions. We have used a 3-D global chemical transport model, driven by meteorological
24 reanalyses and variations in global mean hydroxyl (OH) concentrations derived from CH₃CCl₃
25 observations from two independent networks, to investigate these CH₄ growth variations. The
26 model shows that between 1999 and 2006, changes in the CH₄ atmospheric loss contributed
27 significantly to the suppression in global CH₄ concentrations relative to the pre-1999 trend.
28 The largest factor in this is relatively small variations in global mean OH on a timescale of a
29 few years, with minor contributions of atmospheric transport of CH₄ to its sink region and of
30 atmospheric temperature. Although changes in emissions may be important during the
31 stagnation period, these results imply a smaller variation is required to explain the observed
32 CH₄ trends. The contribution of OH variations to the renewed CH₄ growth after 2007 cannot
33 be determined with data currently available.

34 1. Introduction

35 The global mean atmospheric methane (CH₄) concentration has increased by a factor of 2.5
36 since the pre-industrial era, from approximately 722 ppb in 1750 to 1803.2 ± 0.7 ppb in 2011
37 (Etheridge et al., 1998; Dlugokencky et al., 2005). Over this time period methane has accounted
38 for approximately 20% of the total direct anthropogenic perturbation of radiative forcing by
39 long-lived greenhouse gases (0.48±0.05 W/m²), the second largest contribution after CO₂
40 (Cicerone et al., 1988; Myhre et al., 2013). This long-term methane increase has been attributed
41 to a rise in anthropogenic emissions from fossil fuel exploitation, agriculture, waste
42 management and biomass burning (Dlugokencky et al., 2011). Predictions of future CH₄ levels
43 require a complete understanding of processes governing emissions and atmospheric removal.

44 Since the mid-1980s measurements of CH₄ in discrete atmospheric air samples collected at
45 surface sites have been used to observe changes in the interannual growth rate of CH₄ (Rigby
46 et al., 2008; Dlugokencky et al., 2011, Kirschke et al., 2013). Nisbet et al. (2014) showed that
47 between 1984 and 1992 atmospheric CH₄ increased at ~12 ppb/yr, after which the growth rate
48 slowed to ~3 ppb/yr. In 1999 a period of near-zero growth began which continued until 2007.
49 In 2007 this stagnation period ended and up until 2009 average growth increased again to ~4.9
50 ppb/yr (Rigby et al., 2008; Dlugokencky et al., 2011).

51 The reasons for the pause in CH₄ growth are not well understood. Bousquet et al. (2006)
52 performed an atmospheric transport inversion study to infer an increase in anthropogenic
53 emissions since 1999. Similarly, the EDGAR v3.2, bottom-up anthropogenic emission
54 inventory, an updated inventory to that used as an a priori by Bousquet et al. (2006), shows a
55 year-on-year increase in anthropogenic CH₄ emissions between 1999 and 2006 (Olivier et al.,
56 2005). This would suggest that a decrease in anthropogenic emissions is not the likely cause of
57 the pause in growth during this period. A second potential explanation is a reduction in wetland
58 emissions between 1999 and 2006, which is in part compensated by an increase in
59 anthropogenic emissions (Bousquet et al., 2006). However, more recently, Pison et al. (2013)
60 used two atmospheric inversions alongside a process-based model and found much more
61 uncertainty in the role wetlands played in the pause in growth over this period. Their study
62 found a negative trend in Amazon basin emissions between 2000 and 2006 from the process-
63 based model and a positive trend from the inversion estimates.

64 Dlugokencky et al. (2003) argued that the behaviour of global mean CH₄ up to around 2002
65 was characteristic of the system approaching steady state, accelerated by decreasing emissions
66 at high northern latitudes in the early 1990s and fairly constant emissions elsewhere. However,
67 since then there have been notable perturbations to the balance of sources and sinks (Rigby et
68 al., 2008). The observed growth since 2007 has been, at least partly, attributed to increases in
69 wetland (Bousquet et al., 2011) and anthropogenic emissions (Bousquet et al., 2011). Recent
70 changes in emissions are not well constrained and the reasons for the renewed growth are also
71 not fully understood (Nisbet et al., 2014).

72 Atmospheric chemistry has also been hypothesised to play a role in past variations in CH₄
73 growth rates. The major (90%) sink of atmospheric CH₄ is via reaction with the hydroxyl
74 radical, OH. Variations in the global mean concentration of OH ([OH]), or changes to the

75 reaction rate through changes in temperature, therefore have the potential to affect CH₄ growth.
76 Previous studies have suggested that an increase in atmospheric OH concentration may have
77 been at least partly responsible for a decrease in the CH₄ growth rate (Karlsdottir and Isaksen
78 et al., 2000; Lelieveld et al., 2004; Wang et al., 2004; Fiore et al., 2006). This rise in OH has
79 been attributed to an increase in lightning NO_x (Fiore et al., 2006), a decrease in column O₃
80 (Wang et al., 2004) and changes in atmospheric pollutants (Karlsdottir and Isaksen et al., 2000).
81 The abundance of other species such as H₂O and CH₄ also determine the concentration of OH
82 (Lelieveld et al., 2004). Prinn et al. (2005) and Voulgarakis et al. (2015) suggested that major
83 global wildfires and El Nino Southern Oscillation (ENSO) events could influence [OH]
84 variability.

85 Warwick et al. (2002) investigated the impact of meteorology on atmospheric CH₄ growth rates
86 from 1980 to 1998, i.e. well before the observed recent pause. They concluded that atmospheric
87 conditions could be an important driver in the interannual variability (IAV) of atmospheric
88 CH₄. In similar studies a combination of atmospheric dynamics and changes in emissions were
89 shown to explain some of the earlier past trends in atmospheric CH₄ (Fiore et al., 2006; Patra
90 et al., 2009). This paper builds on these studies to investigate the chemical and non-chemical
91 atmospheric contribution to the recent variations in CH₄ growth. By ‘non-chemical’ we mean
92 transport-related influences, although the loss of CH₄ is ultimately due to chemistry as well.
93 We use a 3-D global chemical transport model to simulate the period from 1993 to 2011 and
94 to quantify the impact of variations in [OH] and meteorology on atmospheric CH₄ growth.

95 **2. Data and Models**

96 **2.1 NOAA and AGAGE CH₄ Data and Derived OH**

97 We have used surface CH₄ observations from 19 National Oceanographic and Atmospheric
98 Administration/Earth System Research Laboratory (NOAA/ESRL) cooperative global air
99 sampling sites (Dlugokencky et al., 2014) over 1993-2009 (see Table 1). To calculate the global
100 average concentration, measurements were interpolated across 180 latitude bins, which were
101 then weighted by surface area. We have also used the same method to derive global mean CH₄
102 based on 5 sites from the Advanced Global Atmospheric Gases Experiment (AGAGE) network
103 (Prinn et al., 2000; Cunnold et al., 2002; Prinn et al., 2015).

104 Montzka et al. (2011) used measurements of methyl chloroform (CH₃CCl₃) from an
105 independent set of flasks sampled approximately weekly at a subset of NOAA air sampling
106 sites to derive global [OH] anomalies from 1997 to 2007 and found only a small interannual
107 variability ($2.3 \pm 1.5\%$). They argued that uncertainties in emissions are likely to limit the
108 accuracy of the inferred inter-annual variability in global [OH], particularly before 1997. At
109 that time the emissions were large but decreasing rapidly due to the phaseout of CH₃CCl₃
110 production and consumption, and the large atmospheric gradients were also more difficult to
111 capture accurately with only few measurement sites. Instrument issues caused an interruption
112 to their CH₃CCl₃ time series in 2008/9. We have averaged these (based on the red curve in
113 Figure 3 of Montzka et al.) into yearly anomalies to produce relative interannual variations in
114 the mean [OH]. Similarly, Rigby et al. (2013) used CH₃CCl₃ measurements from on-site
115 instrumentation operated continuously within the 5-station AGAGE network in a 12-box model

116 to produce yearly global [OH] anomalies from 1995 (the date from which data from all 5
117 stations is available) to 2010. These two timeseries, which convert anomalies in the CH₃CCl₃
118 decay rate into anomalies in [OH] using constant temperature, correspond to the best estimate
119 of [OH] variability from the two measurement networks by the groups who operate them. We
120 then applied these two series of yearly global anomalies uniformly to the global latitude-height
121 [OH] field used in the recent TransCom CH₄ model intercomparison (see Patra et al., 2011),
122 which itself was derived from a combination of semi-empirically calculated tropospheric OH
123 distributions (Spivakovsky et al. 2000; Huijnen et al., 2010) and 2-D model simulated
124 stratospheric loss rates (Velders, 1995). For consistency between the model experiments, both
125 sets of yearly anomalies were scaled so that the mean [OH] between 1997 and 2007 (the overlap
126 period where NOAA and AGAGE anomalies are both available) equalled the TransCom [OH]
127 value. In the rest of this paper we refer to these two OH datasets as ‘NOAA-derived’ and
128 ‘AGAGE-derived’.

129 These two calculations of yearly [OH] anomalies use slightly different assumptions for
130 CH₃CCl₃ emissions after 2002. Before that year they use values from Prinn et al. (2005). The
131 NOAA data then assumed a 20% decay in emission for each subsequent year (Montzka et al.,
132 2011), while AGAGE used United Nations Environment Programme (UNEP) consumption
133 values (UNEP, 2015). Holmes et al. (2013) suggested that inconsistencies in CH₃CCl₃
134 observations between the AGAGE and NOAA networks also limit understanding of OH
135 anomalies for specific years due to an unexplained phasing difference of up to around 3 months.
136 As we are interested in the impact of [OH] changes over longer time periods (e.g. 2000 – 2006),
137 this phase difference will be less important. We have investigated the impact of the different
138 CH₃CCl₃ observations and assumed emissions on the derived [OH] anomalies (see Section
139 3.1).

140 **2.2 TOMCAT 3-D Chemical Transport Model**

141 We have used the TOMCAT global atmospheric 3-D off-line CTM (Chipperfield, 2006) to
142 model atmospheric CH₄ and CH₃CCl₃ concentrations. The TOMCAT simulations were forced
143 by winds and temperatures from the 6-hourly European Centre for Medium-Range Weather
144 Forecasts (ECMWF) ERA-Interim reanalyses (Dee et al., 2011). They covered the period 1993
145 to 2011 with a horizontal resolution of 2.8° × 2.8° and 60 levels from the surface to ~60 km.

146 The TOMCAT simulations use annually repeating CH₄ emissions, which have been scaled to
147 previous estimates of 553 Tg/yr (Ciais et al., 2013), taken from various studies (Fiore et al.,
148 2006; Curry et al., 2007; Bergamaschi et al., 2009; Pison et al., 2009; Spahni et al., 2011; Ito
149 et al., 2012). Annually-repeating anthropogenic emissions (except biomass burning) were
150 calculated from averaging the EDGAR v3.2 (2009) inventory from 1993 to 2009 (Olivier and
151 Berowski, 2001). Biomass burning emissions were calculated using the GFED v3.1 inventory
152 and averaged from 1997 to 2009 (van der Werf et al., 2010). The Joint UK Land Environment
153 Simulator (JULES) (Best et al., 2011; Clark et al., 2011; Hayman et al., 2014) was used to
154 calculate a wetland emission inventory between 1993 and 2009, which was then used to
155 produce a mean annual cycle. Annually-repeating rice (Yan et al., 2009), hydrate, mud volcano,
156 termite, wild animal and ocean (Matthews et al., 1987) emissions were taken from the

157 TransCom CH₄ study (Patra et al., 2011). The methane loss fields comprised an annually
158 repeating soil sink (Patra et al., 2011), an annually repeating stratospheric loss field (Velders,
159 1995) and a specified zonal mean [OH] field. This does not account for longitudinal variations
160 in [OH], which are considered to be negligible compared to latitudinal variations. To create a
161 reasonable spatial distribution the model was spun up for 15 years prior to initialising the
162 simulations, using emission data from 1977 to 1992 where available and annual averages
163 otherwise. Before reinitialising the model in 1993, concentrations were scaled using the model
164 and observed global concentrations to remove any imbalance.

165 Fifteen TOMCAT simulations were performed each with a CH₄ tracer and a CH₃CCl₃ tracer.
166 The runs had differing treatments of meteorology (winds and temperature) and [OH] (see Table
167 2). Simulations with repeating [OH] fields (RE_xxxx) used the TransCom dataset. The other
168 runs with varying [OH] used the NOAA-derived or AGAGE-derived [OH] fields based on the
169 original published work or our estimates (see Section 3.1). For these runs, the mean [OH] field
170 is used where the respective NOAA or AGAGE-derived [OH] is unavailable or uncertain
171 (before 1997 / after 2007 for NOAA and before 1997 / after 2009 for AGAGE). The five
172 simulations with fixed wind and temperature fields (with labels ending in FTFW) used the
173 ERA-Interim analyses from 1996 repeated for all years. The five simulations with varying
174 winds and fixed temperature (with labels ending in FTVW) used zonal mean temperature fields
175 averaged from 1993-2009, any influence from the relatively small longitudinal temperature
176 variations is unlikely to have a noticeable impact. We also derive our own [OH] anomalies
177 from the anomaly in the CH₃CCl₃ loss rate, which combines variations in atmospheric OH
178 concentration with variations in temperature which affect the rate constant of the CH₃CCl₃ +
179 OH reaction. To quantify the importance of this temperature effect we also performed 5 model
180 runs which allow both winds and temperature to vary interannually according to ERA-Interim
181 data (labels ending VTVW). Fixed temperature simulations are used for general analysis
182 because the derived OH anomalies already implicitly contain temperature variations.

183 **3. Results**

184 **3.1 Correlation of CH₄ variations with OH and temperature**

185 We first investigate the extent to which variations in the observed CH₄ growth rate correlate
186 with variations in derived [OH]. Figure 1a shows the published NOAA-derived and AGAGE-
187 derived global [OH] anomalies along with the annual CH₄ growth rate estimated from the
188 NOAA and AGAGE measurements. The two [OH] series show the similar behaviour of
189 negative anomalies around 1997 and 2006/7, and an extended period of more positive
190 anomalies in between. For the time periods covered by the NOAA (1997-2007) and AGAGE
191 (1997-2009) CH₃CCl₃ observations, the two derived [OH] timeseries show negative
192 correlations with the CH₄ growth from NOAA (regression coefficient, R = -0.32) and AGAGE
193 (R = -0.64). Only the AGAGE [OH] correlation, from the longer timeseries, is statistically
194 significant at the 90% level. This correlation could be the result of a bidirectional effect,
195 whereby decreased CH₄ acts to increase [OH]; however, Spivakovsky et al. (2000) showed a
196 25% (~450 ppb) change in model CH₄ equates to a 5-6% change in [OH]. This far exceeds the
197 annual growth observed, therefore this effect is assumed to be small.

198 We can use a simple ‘global box model’ (see Supplement S1) to estimate the [OH] variations
199 required to fit the observed CH₄ growth rate variations assuming constant CH₄ emissions and
200 temperature (black line in Figure 1b). This provides a crude guide to the magnitude of OH
201 variations which could be important for changes in the CH₄ budget. Our results are consistent
202 with those of Montzka et al. (2011) who performed a similar analysis on the NOAA CH₄ data.
203 The required [OH] rarely exceeds their CH₃CCl₃-derived interannual variability (IAV) range
204 of [OH] ($\pm 2.3\%$, shown as shading in the figure). Also shown in Figure 1b are the published
205 estimates of the global mean OH anomalies from Figure 1a, converted to concentration units
206 (see Section 2.1). The relative interannual variations in [OH] required to fit the CH₄
207 observations match the CH₃CCl₃-derived [OH] variations in many years, for example from
208 1998-2002 (see Montzka et al., 2011). Some of the derived variations in [OH] exceed that
209 required to match the CH₄ growth rate, with larger negative anomalies in the early and later
210 years and some slightly larger positive values in middle of the period.

211 Figures 1c and 1d show our estimates of [OH] using NOAA and AGAGE observations and
212 two assumptions of post-2000 CH₃CCl₃ emissions (see Section 2.1) in a global box model. The
213 figures also compare our OH estimates with the NOAA-derived and AGAGE-derived [OH]
214 anomalies based on the work of the observation groups (Figure 1a). Our results demonstrate
215 the small impact of using different observations and post-2000 emission assumptions (compare
216 filled and open red circles for the two panels). For these box model results there is also only a
217 very small effect of using annually varying temperature (compare red and blue lines). In later
218 years the choice of observations has a bigger impact than the choice of emissions on the derived
219 [OH]. For AGAGE-derived values (Figure 1d) our estimates agree well with the published
220 values of Rigby et al., (2013), despite the fact we use a global box model while they used a
221 more sophisticated 12-box model. In contrast, there are larger differences between our values
222 and the NOAA-derived OH variability published by Montzka et al. (2011) (Figure 1c), despite
223 both studies using box models. In particular, around 2002-2003 we overestimate the positive
224 anomaly in [OH]. We also estimate a much more negative OH anomaly in 1997 than Montzka
225 et al., though we slightly underestimate the published AGAGE-derived anomaly in that year
226 (Figure 1d). Tests show that differences between our results and the NOAA box model are due
227 to the treatment of emissions. This suggests a larger uncertainty in the inferred low 1997 [OH]
228 value, when emissions of CH₃CCl₃ were decreasing rapidly, although reasons why atmospheric
229 [OH] might have been anomalously low were discussed by Prinn et al. (2005). In the subsequent
230 analysis we use the OH variability from the published NOAA and AGAGE studies as input to
231 the 3-D model.

232 **3.2 TOMCAT Simulations**

233 Overall, Figure 1 shows the potential importance of small, observationally derived variations
234 in OH concentrations to impact methane growth. We now investigate this quantitatively in the
235 framework of a 3-D CTM.

236 **3.2.1 Methyl Chloroform**

237 The TOMCAT simulations include a CH₃CCl₃ tracer. This allows us to verify that our approach
238 of using a global OH field, scaled by derived anomalies, allows the model to reproduce the
239 observed magnitude and variability of CH₃CCl₃ decay accurately. Figure 2a shows that the

240 model, with the imposed [OH] field, does indeed simulate the global decay of CH₃CCl₃ very
241 well. This justifies our use of the ‘offline’ [OH] field, as models with interactive tropospheric
242 chemistry can produce a large range in absolute global mean [OH] and therefore in lifetimes
243 of gases such as CH₃CCl₃. For example, Voulgarakis et al., (2013) analysed the global mean
244 [OH] from various 3D models and found a range of 0.65×10^6 to 1.34×10^6 molecules cm⁻³.
245 Furthermore, Montzka et al., (2011) discussed how photochemical models typically show
246 smaller interannual variability than CH₃CCl₃-derived OH, again suggesting that the models are
247 not accurately capturing all relevant processes. Figure 2a also shows that the global mean
248 CH₃CCl₃ from the NOAA and AGAGE networks differ by ~2.5ppt around 1993-1996, but
249 since then this difference has become smaller.

250 The observed and modelled CH₃CCl₃ decay rate anomalies (calculated using the method of
251 Holmes et al., (2013) with a 12-month smoothing) are shown in Figures 2b and 2c (different
252 panels are used for AGAGE and NOAA comparisons for clarity). The model and observation-
253 derived results both tend to show a faster CH₃CCl₃ decay (more positive anomaly) in the middle
254 of the period, with slower decay at the start and end. The anomalies for the NOAA and
255 AGAGE-derived OH show periodic variations on a timescale of 2-3 yrs but with a phase shift
256 between the two datasets of 3 months, as noted by Holmes et al., (2013). The model runs with
257 OH variability prescribed from the observations and varying winds also show these periodic
258 variations with correlation coefficients ranging from 0.71 – 0.90. The correlation values for
259 these runs using varying OH are all larger than the run using repeating OH (for RE_FTVW
260 R=0.62 compared to AGAGE data and 0.67 compared to NOAA data). Note that for CH₃CCl₃
261 decay there are only small differences between the 3-D simulations which use varying
262 temperatures and the corresponding runs which use fixed temperature (e.g. simulation
263 RE_VTVW versus RE_FTVW). This agrees with the results of Montzka et al (2011) based on
264 their box model. This shows that the largest contribution from the CH₃CCl₃ decay rate anomaly
265 comes from variations in atmospheric OH concentration, rather than atmospheric temperature.
266 The simulations with repeating winds show less variability in the CH₃CCl₃ decay rate,
267 particularly in the period 1999-2004, but the small difference suggests that the interannual
268 variability in the observed CH₃CCl₃ decay rate is driven primarily by the variations in the OH
269 concentration. The remaining interannual variability in run RE_FTVW is due to variations in
270 emissions.

271 Figure 3 shows the CH₃CCl₃ decay and decay rate anomalies at four selected stations, two from
272 the NOAA network and two from the AGAGE network. The good agreement in the global
273 CH₃CCl₃ decay in Figure 2 is also seen at these individual stations. At the AGAGE stations of
274 Mace Head and Gape Grim, the model runs with varying OH perform better in capturing the
275 decay rate anomalies than the runs with repeating OH. However, the impact of variability in
276 the winds (solid lines versus dotted lines) is more apparent at these individual stations
277 compared to the global means. At the NOAA station of Mauna Loa the model run with varying
278 OH and varying winds also appears to perform better in capturing the observed variability in
279 CH₃CCl₃ decay. At the South Pole the observed variability is small, except in 2000-2002. This
280 feature is not captured by the model.

281 In summary, Figures 2 and 3 show that the global OH fields that we have constructed from
282 different datasets can perform well in capturing the decay of CH₃CCl₃ and its anomalies both
283 globally and at individual stations. Although, the interannual variability in global mean OH has
284 been derived from these CH₃CCl₃ observations, the figures do show that the reconstructed
285 model OH fields (which also depend on the methodology discussed in Section 2) perform well
286 in simulating CH₃CCl₃ within the 3D model. Therefore, we would argue that these fields are
287 suitable for testing the impact of OH variability on the methane growth rate. Even so, it is
288 important to bear in mind that these fields may not represent the true changes in atmospheric
289 OH, particularly if the interannual variability in CH₃CCl₃ emissions was a lot different to that
290 assumed here. However, we would again note that we are focussing on the impact of multi-
291 year (≥ 2 years) variability which appears more robustly determined by the networks under
292 differing assumptions of temperature and emissions than year-to-year variability.

293

294 **3.2.2 Methane**

295 Figure 4 shows deseasonalised modelled surface CH₄ from the 3-D CTM simulations compared
296 with in-situ observations from a northern high-latitude station (Alert), two tropical stations
297 (Mauna Loa and Tutuila), a southern high-latitude station (South Pole) and the global average
298 of the NOAA and AGAGE stations. The global comparisons are shown for simulations both
299 with varying and repeating meteorology. Figure 5 shows the global annual CH₄ growth rates
300 with a 12-month smoothing (panel a) and differences between the model and NOAA and
301 AGAGE observations (panels b and c). The changes in the modelled global mean CH₄ over
302 different time periods are given in Table 3.

303 Figure 4 shows that in 1993, at the end of the model spin-up, the simulations capture the global
304 mean CH₄ level well, along with the observed values at a range of latitudes. The exception is
305 at high northern latitudes. However, these differences are not important when investigating the
306 change in the global growth rate. The global change in atmospheric CH₄ in all simulations from
307 1993 to the end of 2009 is between 75 and 104 ppb, compared to 56 and 66 ppb in the
308 observations.

309 Model run RE_FTFW does not include interannual variations in atmospheric transport or CH₄
310 loss. Therefore, and also given the lack of change in emissions the modelled CH₄ gradually
311 approaches a steady state value of ~1830 ppb (Figure 4f). The rate of CH₄ growth decreases
312 from 7.9 ppb/yr (1993-1998) to 1.4 ppb/yr (2007-2009). Compared to run RE_FTFW, the other
313 simulations introduce variability on this CH₄ evolution.

314 Run RE_FTVW includes interannual variability in wind fields which may alter the transport
315 of CH₄ from the source (emission) to the sink regions. The largest difference between runs
316 RE_FTFW and RE_FTVW occurs after 2000 (Figure 4f). During the stagnation period (1999-
317 2006) run RE_FTVW has a smaller growth rate of 3.5 ppb/yr compared to 4.1 ppb/yr in run
318 RE_FTFW, showing that variations in atmospheric transport made a small contribution to the
319 slowdown in global mean CH₄ growth.

320 Compared to run RE_FTVW, runs AP_FTVW, AL_FTVW, NP_FTVW and NL_FTVW
321 include CH₃CCl₃-derived interannual variations in [OH] which introduce large changes in

322 modelled CH₄, which are more in line with the observations (Figure 4e and 5). These runs
323 produce turnarounds in the CH₄ growth in 2001/2 (becomes negative) and 2005/6 (returns to
324 being positive). For AGAGE-derived [OH] (runs AP_FTVW, AL_FTVW) the large negative
325 anomaly in OH in 1997 produces a significant increase in CH₄ prior to the turnround in 2001.

326 Table 3 summarises the change in global mean CH₄ over different time periods. These periods
327 are defined by the key dates in the observed record, i.e. 1999 and 2006 as the start and end
328 dates of the stagnation period. Comparison of Figure 4e and Table 3 shows, however, that the
329 timing of the largest modelled change in growth rate do not necessarily coincide with those
330 dates. That is understandable if other factors not considered here, e.g. emission changes, are
331 contributing to the change in global CH₄ concentration. It does mean that the summary model
332 values in Table 3 do not capture the full impact of the changes in [OH] and winds within the
333 stagnation period. Figure 4e shows that model runs with varying OH perform better in
334 simulating the relative CH₄ trend from 1999 to around 2004.

335 Table 3 shows that runs NP_FTVW and NL_FTVW (NOAA-derived [OH]) produce a small
336 modelled CH₄ growth of 2.5-3.1 ppb/yr during the stagnation period 1999-2006, compared to
337 1.0 ppb/yr for run AP_FTVW (AGAGE-derived [OH]). The AGAGE results are slightly larger
338 than the observed growth rate of 0.6-0.7 ppb/yr. Runs AL_FTVW, AP_FTVW, NL_FTVW
339 and NP_FTVW capture the observed strong decrease in the CH₄ growth rate. With the
340 exception of AP_FTVW between 1999 and 2006 (p-value = 0.37) all trends, over all three time
341 periods, are statistically significant at the 90% level. Clearly, these runs demonstrate the
342 significant potential for relatively small variations in mean [OH] to affect CH₄ growth.
343 Excluding the stagnation period the mean modelled CH₄ lifetime in run NP_FTVW is 9.4 years,
344 but this decreases slightly by 0.01 years during the stagnation period. For run AP_FTVW there
345 is a decrease of 0.18 years from 9.6 years between the same intervals. The results from all the
346 CTM simulations during 1999-2006 indicate that the accuracy of modelled CH₄ growth is
347 improved by accounting for interannual variability in [OH] as derived from CH₃CCl₃
348 observations, and interannual variability in meteorology.

349 The variation of [OH] after 2007 cannot be determined from the available NOAA data so run
350 NP_FTVW used the mean [OH] field for all subsequent years. The modelled CH₄ increase of
351 3.5 ppb/yr underestimates the observations (4.9 ppb/yr). Should the lower [OH] of 2007 have
352 persisted then the model would have produced a larger increase in CH₄, in better agreement
353 with the observations. The AGAGE-derived [OH] for 2007-2009 (run AP_FTVW) produces a
354 larger CH₄ growth relative to the previous years (8.8 ppb/yr). Runs RE_FTFW (1.4 ppb/yr) and
355 RE_FTVW (1.8 ppb/yr) both show a decreased rate of growth during the final 5 years,
356 consistent with a system approaching steady state.

357 Figure 5a shows the global CH₄ growth rate derived from the AGAGE and NOAA networks
358 together with selected model simulations. Figures 5b and c show the differences between the
359 model simulations and the NOAA and AGAGE observations, respectively. The runs which
360 include variations in [OH] agree better with the observed changes, i.e. larger R values in panel
361 (a) and the model lines are closer to the y=0 line in panels (b) and (c), especially in the first 5
362 years of the stagnation period. It is interesting to note that the relative impacts of wind and
363 temperature variations are larger for CH₄ than for CH₃CCl₃ (compare simulations RE_FTFW,

364 RE_FTVW and RE_VTVW in Figures 2 and 5a). The temperature dependences of the OH loss
365 reactions are similar for the two species (see Supplement S1) but the impact of transport from
366 emission regions to chemical loss regions is more variable for CH₄. One possibility for this is
367 differences in the spatial distribution of CH₄ and CH₃CCl₃ emissions. This needs to be
368 considered when applying results derived from CH₃CCl₃ to CH₄.

369 **4. Discussion and Conclusions**

370 Our model results suggest that variability in atmospheric [OH] played a key role in the observed
371 recent variations in CH₄ growth, particularly during the CH₄ stagnation period between 1999
372 and 2006. The 3-D CTM calculations show that during the stagnation period, variations in
373 atmospheric conditions in the tropical lower to mid-troposphere could potentially account for
374 an important component of the observed decrease in global CH₄ growth. Within this, small
375 increases in [OH] were the largest factor, while variations in transport from source to sink
376 regions made a smaller contribution. Note again, however, that the ultimate loss of CH₄ is still
377 due to chemistry. The role of atmospheric temperature variations is factored into the
378 observationally derived OH, but model experiments show that changes in the OH concentration
379 itself is most important. The remainder of the variation can be ascribed to other processes not
380 considered in our runs such as emission changes. There are also measurement uncertainties to
381 consider and the possible underrepresentation of the global mean CH₃CCl₃ which will affect
382 the derived OH concentration. Our results are consistent with an earlier budget study which
383 analysed 1991 to 2004 and found that variations in [OH] were the main control of variations in
384 atmospheric CH₄ lifetime (65%), with temperature accounting for a smaller fraction (35%)
385 (Fiore et al., 2006). However, they were not able to study the full period of the pause in CH₄
386 growth and did not impose observation-based [OH] variations. As we have noted here the
387 CH₄ lifetime can also be affected by emissions distributions which affects transport to the main
388 loss regions.

389 Prior to the stagnation period the simulation using AGAGE-derived [OH] (9.7-10.4 ppb/yr)
390 overestimates CH₄ growth when compared to observations (6.0-7.1 ppb/yr), which degrades
391 the agreement with the observed CH₄ variations. A likely cause of this is inaccuracies in derived
392 [OH] in 1997 when emissions still played a large role in the observed CH₃CCl₃ and the e-fold
393 decay had not yet stabilised (Montzka et al., 2011).

394 We have not accounted for expected variations in CH₄ emissions in this study. We can conclude
395 that although global CH₄ emissions do vary year-to-year, the observed trend in CH₄ growth
396 between 1999 and 2006 was impacted by changing atmospheric processes that affected CH₄
397 loss. Changes in emissions are still important over this time period and likely still dominate
398 CH₄ variations over other time periods. The observed changes in growth rates during ENSO
399 events in e.g. 1998 are poorly captured by the meteorological changes considered here and can
400 be attributed to changes in emissions through changing precipitation and enhanced biomass
401 burning (Hodson et al., 2011). The renewed growth of CH₄ in 2007 is also poorly captured by
402 all model simulations without varying [OH]. The observed decrease in AGAGE and NOAA-
403 derived [OH] coincides with the increase in CH₄ growth in 2007, although the currently

404 available data do not allow for a more detailed investigation of the possible contribution of
405 [OH] changes in this recent increase.

406 Despite the differences in year-to-year variability in [OH] derived from CH₃CCl₃ observations
407 (Holmes et al., 2013), we find that [OH] variability derived from two different networks of
408 surface CH₃CCl₃ observations over multi-year periods provide insights into atmospheric CH₄
409 variations. Improved quantification of the role of OH variability will require efforts to reduce
410 uncertainties associated with estimating [OH]. Estimates of global mean [OH] in recent years
411 from CH₃CCl₃ observations are becoming increasingly difficult because CH₃CCl₃ levels are
412 currently <5 ppt; hence this may limit the accuracy of derived [OH] and its variability in future
413 years (Lelieveld et al., 2006). Wennberg et al. (2004) also noted that there can be time
414 variations in the net flux of CH₃CCl₃ by the oceans, which could potentially affect the derived
415 [OH] concentrations and which were not considered in our analysis. However, the impact of
416 interannual variability in this flux are not likely to be important. For the period considered in
417 this study, Figure 2 of Wennberg et al., (2004) shows that the CH₃CCl₃ flux into the ocean
418 decreased from the largest value in 1997 to almost zero in recent years, which mimics CH₃CCl₃
419 emissions. Including the estimated 1997 ocean flux in our box model decreased the OH
420 anomaly for that year by 0.8%. This change would decrease in magnitude in the subsequent
421 years. Overall, accurate estimates of [OH] beyond 2009 will require more sophisticated
422 analysis of CH₃CCl₃ observations, derivation from other species or improved representation
423 of [OH] in photochemical models.

424 Overall our study suggests that future atmospheric trends in CH₄ are likely to be strongly
425 influenced by not only emissions but also by changes in processes that affect atmospheric loss.
426 . Therefore, to be realistic, predictions of these future trends need to explicitly account for likely
427 variations in [OH], the major sink, and possibly other processes related to tropospheric and
428 stratospheric chemistry.

429 **Acknowledgements:** JRM thanks NERC National Centre for Earth Observation (NCEO) for
430 a studentship. CW, MPC and MG acknowledge support from NERC grants GAUGE
431 (NE/K002244/1) and AMAZONICA (NE/F005806/1). GDH acknowledges support from the
432 European Space Agency through its Support to Science Element initiative (ALANIS Methane),
433 NCEO and the NERC MAMM grant (NE/I028327/1). SAM acknowledges support in part from
434 NOAA Climate Program Office's AC4 program. AGAGE is supported by NASA grants
435 NNX11AF17G to MIT and NNX11AF15G and NNX11AF16G to SIO, by NOAA, UK
436 Department of Food and Rural Affairs (DEFRA) and UK Department for Energy and Climate
437 Change (DECC) grants to Bristol University, and by CSIRO and Australian Bureau of
438 Meteorology. MR is supported by a NERC Advanced Fellowship (NE/I021365/1). Model
439 calculations were performed on the Arc1 and Archer supercomputers.

440 **References**

- 441 Bergamaschi, P., Frankenberg, C., Meirink, J. F., Krol, M., Villani, M. G., Houweling, S.,
442 Dentener, F., Dlugokencky, E. J., Miller, J. B., Gatti, L. V., Engel, A., and Levin, I.:
443 Inverse modeling of global and regional CH₄ emissions using SCIAMACHY satellite
444 retrievals, *J. Geophys. Res.*, 114, 10.1029/2009jd012287, 2009.
- 445 Best, M. J., Pryor, M., Clark, D. B., Rooney, G. G., Essery, R. L. H., Ménard, C. B.,
446 Edwards, J. M., Hendry, M. A., Porson, A., Gedney, N., Mercado, L. M., Sitch, S.,
447 Blyth, E., Boucher, O., Cox, P. M., Grimmond, C. S. B., and Harding, R. J.: The Joint
448 UK Land Environment Simulator (JULES), model description – Part 1: Energy and
449 water fluxes, *Geosci. Model Dev.*, 4, 677-699, 10.5194/gmd-4-677-2011, 2011.
- 450 Bousquet, P., Ciais, P., Miller, J. B., Dlugokencky, E. J., Hauglustaine, D. A., Prigent, C.,
451 Van der Werf, G. R., Peylin, P., Brunke, E. G., Carouge, C., Langenfelds, R. L.,
452 Lathiere, J., Papa, F., Ramonet, M., Schmidt, M., Steele, L. P., Tyler, S. C., and White,
453 J.: Contribution of anthropogenic and natural sources to atmospheric methane
454 variability, *Nature*, 443, 439-443, 10.1038/nature05132, 2006.
- 455 Bousquet, P., Ringeval, B., Pison, I., Dlugokencky, E. J., Brunke, E. G., Carouge, C.,
456 Chevallier, F., Fortems-Cheiney, A., Frankenberg, C., Hauglustaine, D. A., Krummel,
457 P. B., Langenfelds, R. L., Ramonet, M., Schmidt, M., Steele, L. P., Szopa, S., Yver, C.,
458 Viovy, N., and Ciais, P.: Source attribution of the changes in atmospheric methane for
459 2006–2008, *Atmos. Chem. Phys.*, 11, 3689-3700, 10.5194/acp-11-3689-2011, 2011.
- 460 Chipperfield, M. P.: New version of the TOMCAT/SLIMCAT off-line chemical transport
461 model: Intercomparison of stratospheric tracer experiments. *Q. J. R. Meteorol Soc.*,
462 132, 1179–1203, 2006.
- 463 Ciais, P., Sabine, C., Bala, G., Bopp, L., Brovkin, V., Canadell, J., Chhabra, A., DeFries, R.,
464 Galloway, J., Heimann, M., Jones, C., Le Quere, C., Myneni, R. B., Piao, S., and
465 Thornton, P.: Carbon and other biogeochemical cycles, in: *Climate Change 2013: The*
466 *Physical Science Basis. Contribution of Working Group I to the Fifth Assessment*
467 *Report of the Intergovernmental Panel on Climate Change*, Cambridge University
468 Press, 2013.
- 469 Cicerone, R. J., and Oremland, R. S.: Biogeochemical aspects of atmospheric methane,
470 *Global Biogeochem. Cycles*, 2, 299-327, 1988.
- 471 Clark, D. B., Mercado, L. M., Sitch, S., Jones, C. D., Gedney, N., Best, M. J., Pryor, M.,
472 Rooney, G. G., Essery, R. L. H., Blyth, E., Boucher, O., Harding, R. J., Huntingford,
473 C., and Cox, P. M.: The Joint UK Land Environment Simulator (JULES), Model
474 description – Part 2: Carbon fluxes and vegetation, *Geosci. Model Dev.*, 4, 701-722,
475 10.5194/gmd-4-701-2011, 2011.
- 476 Cunnold, D., Steele, L., Fraser, P., Simmonds, P., Prinn, R., Weiss, R., Porter, L., O'Doherty,
477 S., Langenfelds, R., and Krummel, P.: In situ measurements of atmospheric methane at
478 GAGE/AGAGE sites during 1985–2000 and resulting source inferences, *J. Geophys.*
479 *Res.*, 107, ACH 20-21-ACH 20-18, 2002.
- 480 Curry, C. L.: Modeling the soil consumption of atmospheric methane at the global scale,
481 *Global Biogeochem. Cycles*, 21, GB4012, doi:10.1029/2006GB002818, 2007.

482 Dee, D., Uppala, S., Simmons, A., Berrisford, P., Poli, P., Kobayashi, S., Andrae, U.,
483 Balmaseda, M., Balsamo, G., Bauer, P., et al.: The ERA - Interim reanalysis:
484 Configuration and performance of the data assimilation system, *Q. J. R. Meteorol. Soc.*,
485 137, 553-597, 2011.

486 Dlugokencky, E. J., Houweling, S., Bruhwiler, L., Masarie, K., Lang, P., Miller, J., and Tans,
487 P.: Atmospheric methane levels off: Temporary pause or a new steady - state?,
488 *Geophys. Res. Lett.*, 30, doi:10.1029/2003GL018126, 2003.

489 Dlugokencky, E. J., Myers, R., Lang, P., Masarie, K., Crotwell, A., Thoning, K., Hall, B.,
490 Elkins, J., and Steele, L.: Conversion of NOAA atmospheric dry air CH₄ mole fractions
491 to a gravimetrically prepared standard scale, *J. Geophys. Res.*, 110, D18306, 2005.

492 Dlugokencky, E. J., Nisbet, E. G., Fisher, R., and Lowry, D.: Global atmospheric methane:
493 budget, changes and dangers, *Philos. Trans. R. Soc. A*, 369, 2058-2072,
494 10.1098/rsta.2010.0341, 2011.

495 Dlugokencky, E. J., P.M. Lang, A.M. Crotwell, K.A. Masarie, M.J. Crotwell, Atmospheric
496 Methane Dry Air Mole Fractions from the NOAA ESRL Carbon Cycle Cooperative
497 Global Air Sampling Network, 1983-2013, Version: 2014-06-24. Available at
498 ftp://aftp.cmdl.noaa.gov/data/trace_gases/ch4/flask/surface/. Accessed July 6, 2014.

499 Etheridge, D. M., Steele, L. P., Francey, R. J., and Langenfelds, R. L.: Atmospheric methane
500 between 1000 A.D. and present: Evidence of anthropogenic emissions and climatic
501 variability, *J. Geophys. Res.*, 103, 15,979-15,993, 10.1029/98jd00923, 1998.

502 Fiore, A. M., Horowitz, L. W., Dlugokencky, E. J., and West, J. J.: Impact of meteorology
503 and emissions on methane trends, 1990–2004, *Geophys. Res. Lett.*, 33, L12809,
504 10.1029/2006gl026199, 2006.

505 Hayman, G.D., et al., Comparison of the HadGEM2 climate-chemistry model against in-situ
506 and SCIAMACHY atmospheric methane data, *Atmos. Chem. Phys.*, 14, 13,257-13,280,
507 2014.

508 Hodson, E. L., Poulter, B., Zimmermann, N. E., Prigent, C., and Kaplan, J. O.: The El Niño-
509 Southern Oscillation and wetland methane interannual variability, *Geophys. Res. Lett.*,
510 38, L08810, 10.1029/2011gl046861, 2011.

511 Holmes, C. D., Prather, M. J., Søvde, O., and Myhre, G.: Future methane, hydroxyl, and their
512 uncertainties: key climate and emission parameters for future predictions, *Atmos.*
513 *Chem. Phys.*, 13, 285-302, 2013.

514 Huijnen, V., Williams, J., Weele, M. v., Noije, T. v., Krol, M., Dentener, F., Segers, A.,
515 Houweling, S., Peters, W., and de Laat, J.: The global chemistry transport model TM5:
516 description and evaluation of the tropospheric chemistry version 3.0, *Geosci. Model*
517 *Dev.*, 3, 445-473, 2010.

518 Ito, A., and Inatomi, M.: Use of a process-based model for assessing the methane budgets of
519 global terrestrial ecosystems and evaluation of uncertainty, *Biogeosciences*, 9, 759-773,
520 10.5194/bg-9-759-2012, 2012.

521 Karlsdottir, S. and Isaksen, I.S.A.: Changing methane lifetime: Possible cause for reduced
522 growth. *Geophys. Res. Lett.*, 27(1), 93-96, 2000.

523 Kirschke, S., Bousquet, P., Ciais, P., Saunio, M., Canadell, J. G., Dlugokencky, E. J.,
524 Bergamaschi, P., Bergmann, D., Blake, D. R., Bruhwiler, L., et al.: Three decades of
525 global methane sources and sinks, *Nature Geosci.*, 6, 813-823, 2013.

526 Lelieveld, J., Dentener, F., Peters, W., and Krol, M.: On the role of hydroxyl radicals in the
527 self-cleansing capacity of the troposphere, *Atmos. Chem. Phys.*, 4, 2337-2344, 2004.

528 Lelieveld, J., Brenninkmeijer, C. A. M., Joeckel, P., Isaksen, I. S. A., Krol, M. C., Mak, J. E.,
529 Dlugokencky, E., Montzka, S. A., Novelli, P. C., Peters, W. and Tans, P. P.: New
530 Directions: Watching over tropospheric hydroxyl (OH), *Atmospheric Environment*, 40,
531 5741-5743, 2006.

532 Matthews, E., and Fung I.: Methane emissions from natural wetlands: Global distribution,
533 area, and ecology of sources. *Global Biogeochem. Cycles*, 1, 61–86, 1987.

534 Montzka, S. A., Krol, M., Dlugokencky, E., Hall, B., Jöckel, P., and Lelieveld, J.: Small
535 interannual variability of global atmospheric hydroxyl, *Science*, 331, 67-69, 2011.

536 Myhre, G., Shindell, D., Bréon, F., Collins, W., Fuglestedt, J., Huang, J., Koch, D.,
537 Lamarque, J., Lee, D., Mendoza, B., Nakajima, T., Robock, A., Stephens, G.,
538 Takemura, T., and Zhang, H.: Anthropogenic and natural radiative forcing, in: *Climate*
539 *Change 2013: The Physical Science Basis. Contribution of Working Group I to the*
540 *Fifth Assessment Report of the Intergovernmental Panel on Climate Change*,
541 Cambridge University Press, 2013.

542 Naik, V., Voulgarakis, A., Fiore, A. M., Horowitz, L., Lamarque, J.-F., Lin, M., Prather, M.
543 J., Young, P., Bergmann, D., and Cameron-Smith, P.: Preindustrial to present-day
544 changes in tropospheric hydroxyl radical and methane lifetime from the Atmospheric
545 Chemistry and Climate Model Intercomparison Project (ACCMIP), *Atmos. Chem.*
546 *Phys.*, 13, 5277-5298, 2013.

547 Nisbet, E. G., Dlugokencky, E. J., and Bousquet, P.: Atmospheric science. Methane on the
548 rise - again, *Science*, 343, 493-495, 10.1126/science.1247828, 2014.

549 Olivier, J.G.J., Berdowski J.J.M.: Global emissions sources and sinks, in: *The Climate*
550 *System*, edited by: Berdowski J, Guicherit R, and Heij BJ., IISBN 9058092550, A. A.
551 Balkema Publishers/Swets & Zeitlinger Pub., Lisse, The Netherlands, 33–78, 2001.

552 Olivier, J. G., Van Aardenne, J. A., Dentener, F. J., Pagliari, V., Ganzeveld, L. N., and Peters,
553 J. A.: Recent trends in global greenhouse gas emissions: regional trends 1970–2000 and
554 spatial distribution of key sources in 2000, *Environmental Sciences*, 2, 81-99, 2005.

555 Patra, P. K. , Takigawa, M., Ishijima, K., Choi, B.-C., Cunnold, D., J. Dlugokencky, E.,
556 Fraser, P., J. Gomez-Pelaez, A., Goo, T.-Y., Kim, J.-S., Krummel, P., Langenfelds, R.,
557 Meinhardt, F., Mukai, H., O’Doherty, S., G. Prinn, R., Simmonds, P., Steele, P.,
558 Tohjima, Y., Tsuboi, K., Uhse, K., Weiss, R., Worthy, D., and Nakazawa, T.: Growth
559 rate, seasonal, synoptic, diurnal variations and budget of methane in the lower
560 atmosphere, *J. Meteorol. Soc. Japan*, 87, 635-663, 10.2151/jmsj.87.635, 2009.

561 Patra, P. K., Houweling, S., Krol, M., Bousquet, P., Belikov, D., Bergmann, D., Bian, H.,
562 Cameron-Smith, P., Chipperfield, M. P., and Corbin, K.: TransCom model simulations
563 of CH₄ and related species: linking transport, surface flux and chemical loss with CH₄

564 variability in the troposphere and lower stratosphere, *Atmos. Chem. Phys.*, 11, 12,813-
565 12,837, 2011.

566 Patra, P., Krol, M., Montzka, S., Arnold, T., Atlas, E., Lintner, B., Stephens, B., Xiang, B.,
567 Elkins, J., and Fraser, P.: Observational evidence for interhemispheric hydroxyl-radical
568 parity, *Nature*, 513, 219-223, 2014.

569 Pison, I., Bousquet, P., Chevallier, F., Szopa, S., and Hauglustaine, D.: Multi-species
570 inversion of CH₄, CO and H₂ emissions from surface measurements, *Atmos. Chem.*
571 *Phys.*, 9, 5281-5297, 2009.

572 Pison, I., Ringeval, B., Bousquet, P., Prigent, C., and Papa, F.: Stable atmospheric methane in
573 the 2000s: key-role of emissions from natural wetlands, *Atmos. Chem. Phys.*, 13,
574 11,609-11,623, 10.5194/acp-13-11609-2013, 2013.

575 Prinn, R., Weiss, R., Fraser, P., Simmonds, P., Cunnold, D., Alyea, F., O'Doherty, S.,
576 Salameh, P., Miller, B., and Huang, J.: A history of chemically and radiatively
577 important gases in air deduced from ALE/GAGE/AGAGE, *J. Geophys. Res.*, 105,
578 17,751-17,792, 2000.

579 Prinn, R. G.: Evidence for variability of atmospheric hydroxyl radicals over the past quarter
580 century, *Geophys. Res. Lett.*, 32, L07809, 10.1029/2004gl022228, 2005.

581 Prinn, R.G., R.F. Weiss, P.J. Fraser, P.G. Simmonds, S. O'Doherty, P. Salameh, L. Porter, P.
582 Krummel, R.H.J. Wang, B. Miller, C. Harth, B. Grealley, F.A. Van Woy, L.P. Steele, J.
583 Mühle, G. Sturrock, F.N. Alyea, J. Huang, and D.E. Hartley, The ALE / GAGE
584 AGAGE Network (DB1001), Carbon Dioxide Information Analysis Center (CDIAC),
585 U.S. Department of Energy (DOE), <http://cdiac.esd.ornl.gov/ndps/alegag.html>, 2015.

586 Rigby, M., Prinn, R. G., Fraser, P. J., Simmonds, P. G., Langenfelds, R., Huang, J., Cunnold,
587 D. M., Steele, L. P., Krummel, P. B., and Weiss, R. F.: Renewed growth of atmospheric
588 methane, *Geophys. Res. Lett.*, 35, L22805, 2008.

589 Rigby, M., Prinn, R. G., O'Doherty, S., Montzka, S. A., McCulloch, A., Harth, C. M., Mühle,
590 J., Salameh, P., Weiss, R. F., and Young, D.: Re-evaluation of the lifetimes of the
591 major CFCs and CH₃CCl₃ using atmospheric trends, *Atmos. Chem. Phys.*, 13, 2691-
592 2702, 2013.

593 Sander, S.P., et al., *Chemical Kinetics and Photochemical Data for Use in Atmospheric*
594 *Studies Evaluation Number 17. JPL Publication 10-6*, Jet Propulsion Laboratory,
595 Pasadena, USA, 2011.

596 Spahni, R., Wania, R., Neef, L., van Weele, M., Pison, I., Bousquet, P., Frankenberg, C.,
597 Foster, P. N., Joos, F., Prentice, I. C., and van Velthoven, P.: Constraining global
598 methane emissions and uptake by ecosystems, *Biogeosciences*, 8, 1643-1665,
599 10.5194/bg-8-1643-2011, 2011.

600 Spivakovsky, C., Logan, J., Montzka, S., Balkanski, Y., Foreman-Fowler, M., Jones, D.,
601 Horowitz, L., Fusco, A., Brenninkmeijer, C., and Prather, M.: Three-dimensional
602 climatological distribution of tropospheric OH: Update and evaluation, *J. Geophys.*
603 *Res.*, 105, 8931-8980, 2000.

604 UNEP, The UNEP Environmental Data Explorer, as compiled from United Nations
605 Environment Programme . United Nations Environment Programme.
606 <http://ede.grid.unep.ch>, 2015.

607 van der Werf, G. R., Randerson, J. T., Giglio, L., Collatz, G., Mu, M., Kasibhatla, P. S.,
608 Morton, D. C., DeFries, R., Jin, Y. v., and van Leeuwen, T. T.: Global fire emissions
609 and the contribution of deforestation, savanna, forest, agricultural, and peat fires (1997–
610 2009), *Atmos. Chem. Phys.*, 10, 11707-11735, 2010.

611 Velders, G. J. M.: Description of the RIVM 2-dimensional stratosphere model, RIVM
612 Rapport 722201002, 1995.

613 Voulgarakis, A., Naik, V., Lamarque, J.-F., Shindell, D. T., Young, P., Prather, M. J., Wild,
614 O., Field, R., Bergmann, D., and Cameron-Smith, P.: Analysis of present day and future
615 OH and methane lifetime in the ACCMIP simulations, *Atmos. Chem. Phys.*, 13, 2563-
616 2587, 2013.

617 Voulgarakis, A., Marlier, M.E., Faluvegi, G., Shindell, D.T., Tsigaridis, K. and Mangeon, S.:
618 Interannual variability of tropospheric trace gases and aerosols: The role of biomass
619 burning emissions, *J. Geophys. Res.: Atmos.*, 120(14), 7157-7173, 2015.

620 Wang, J.S., Logan, J.A., McElroy, M.B., Duncan, B.N., Megretskaia, I.A. and Yantosca,
621 R.M.: A 3 - D model analysis of the slowdown and interannual variability in the
622 methane growth rate from 1988 to 1997, *Global Biogeochem. Cycles*, 18(3), 2004.

623 Warwick, N. J., Bekki S., Law K. S., Nisbet E. G., and Pyle, J. A.: The impact of
624 meteorology on the interannual growth rate of atmospheric methane, *Geophys. Res.*
625 *Lett.*, 29, doi:10.1029/2002GL015282, 2002.

626 Wennberg, P. O., Peacock, S., Randerson, J. T., and Bleck, R.: Recent changes in the air -
627 sea gas exchange of methyl chloroform, *Geophys. Res. Lett.*, 31, L16112, 2004.

628 Yan, X., Akiyama, H., Yagi, K., and Akimoto, H.: Global estimations of the inventory and
629 mitigation potential of methane emissions from rice cultivation conducted using the
630 2006 Intergovernmental Panel on Climate Change Guidelines, *Global Biogeochem.*
631 *Cycles*, 23, GB2002, 10.1029/2008gb003299, 2009.

632

633 **Tables**

634

635 **Table 1.** List of NOAA and AGAGE stations which provided CH₄ and CH₃CCl₃ observations.

Site Code	Site Name	Lat. (°N)	Lon. (°N)	Altitude (km)	CH ₄	CH ₃ CCl ₃	Start Date ⁺⁺	End Date
ABP	Arembepe, Brazil	-12.77	-38.17	0	NOAA		27/10/2006	12/01/2010
ALT	Alert, Canada	82.45	-62.51	0.2	NOAA	NOAA	10/06/1985	Ongoing
ASC	Ascension Island, UK	7.97	-14.4	0.09	NOAA		11/05/1983	Ongoing
BRW	Barrow, USA	71.32	-156.61	0.01	NOAA	NOAA	06/04/1983	Ongoing
CGO	Cape Grim, Australia	-40.68	144.69	0.09	NOAA/AGAGE	NOAA/AGAGE	19/04/1984	Ongoing
HBA	Halley Station, UK	-75.61	-26.21	0.03	NOAA		17/01/1983	Ongoing
ICE	Storhofdi, Iceland	63.4	-20.29	0.12	NOAA		02/10/1992	Ongoing
KUM	Cape Kumukahi, USA	19.5	-154.8	0.02	-	NOAA	-	-
LEF	Park Falls, USA	45.9	-90.3	0.47	-	NOAA	-	-
MHD	Mace Head, Ireland	53.33	-9.9	0.01	NOAA/AGAGE	AGAGE**	03/06/1991	Ongoing
MLO	Mauna Loa, USA	19.54	-155.58	3.4	NOAA	NOAA	06/05/1983	Ongoing
NWR	Niwot Ridge, USA	40.05	-105.59	3.52	NOAA	NOAA	21/06/1983	Ongoing
PAL	Pallas-Sammaltunturi, Finland	67.97	24.12	0.56	NOAA		21/12/2001	Ongoing
PSA	Palmer Station, USA	-64.92	-64	0.01	NOAA	**	01/01/1983	Ongoing
RPB	Ragged Point, Barbados	13.17	-59.43	0.02	NOAA/AGAGE	AGAGE	14/11/1987	Ongoing
SEY	Mahe Island, Seychelles	-4.68	55.53	0	NOAA		12/05/1983	Ongoing
SMO	Tutuila, American Samoa	-14.25	-170.56	0.04	NOAA	NOAA/AGAGE	23/04/1983	Ongoing
SPO	South Pole, USA	-89.98	-24.8	2.81	NOAA	NOAA	20/02/1983	Ongoing
STM	Ocean Station M, Norway	66	2	0	NOAA		29/04/1983	27/11/2009
SUM	Summit, Greenland	72.6	-38.42	3.21	NOAA	**	23/06/1997	Ongoing
THD	Trinidad Head, USA	41.1	-124.1	0.1	AGAGE	AGAGE**	09/1995	Ongoing
ZEP	Ny-Alesund, Norway/Sweden	78.91	11.89	0.47	NOAA		11/02/1994	Ongoing

636

637 ++For NOAA CH₃CCl₃ data the record starts in 1992 at 7 of the 9 stations used here. It started
638 in 1995 for KUM and 1996 for LEF.

639 **NOAA flask data from these sites was not used in the present study or in Montzka et al.,
640 (2011).

641 **Table 2.** Summary of the fifteen TOMCAT 3-D CTM simulations.

Run	OH time variation	Meteorology ^b	
		Winds ^c	Temperature ^d
RE_FTFW	Repeating ^a	Fixed	Fixed
RE_FTVW	Repeating ^a	Varying	Fixed
RE_VTVW	Repeating ^a	Varying	Varying
AP_FTFW	AGAGE (Rigby et al., 2013)	Fixed	Fixed
AP_FTVW	AGAGE (Rigby et al., 2013)	Varying	Fixed
AP_VTVW	AGAGE (Rigby et al., 2013)	Varying	Varying
AL_FTVT	AGAGE (this work)	Fixed	Fixed
AL_FTVW	AGAGE (this work)	Varying	Fixed
AL_VTVW	AGAGE (this work)	Varying	Varying
NP_FTFW	NOAA (Montzka et al., 2011)	Fixed	Fixed
NP_FTVW	NOAA (Montzka et al., 2011)	Varying	Fixed
NP_VTVW	NOAA (Montzka et al., 2011)	Varying	Varying
NL_FTFW	NOAA (this work)	Fixed	Fixed
NL_FTVW	NOAA (this work)	Varying	Fixed
NL_VTVW	NOAA (this work)	Varying	Varying

642 a. Annually repeating [OH] taken from Patra et al. (2011).

643 b. Varying winds and temperatures are from ERA-Interim.

644 c. Fixed winds using repeating ERA-Interim winds from 1996.

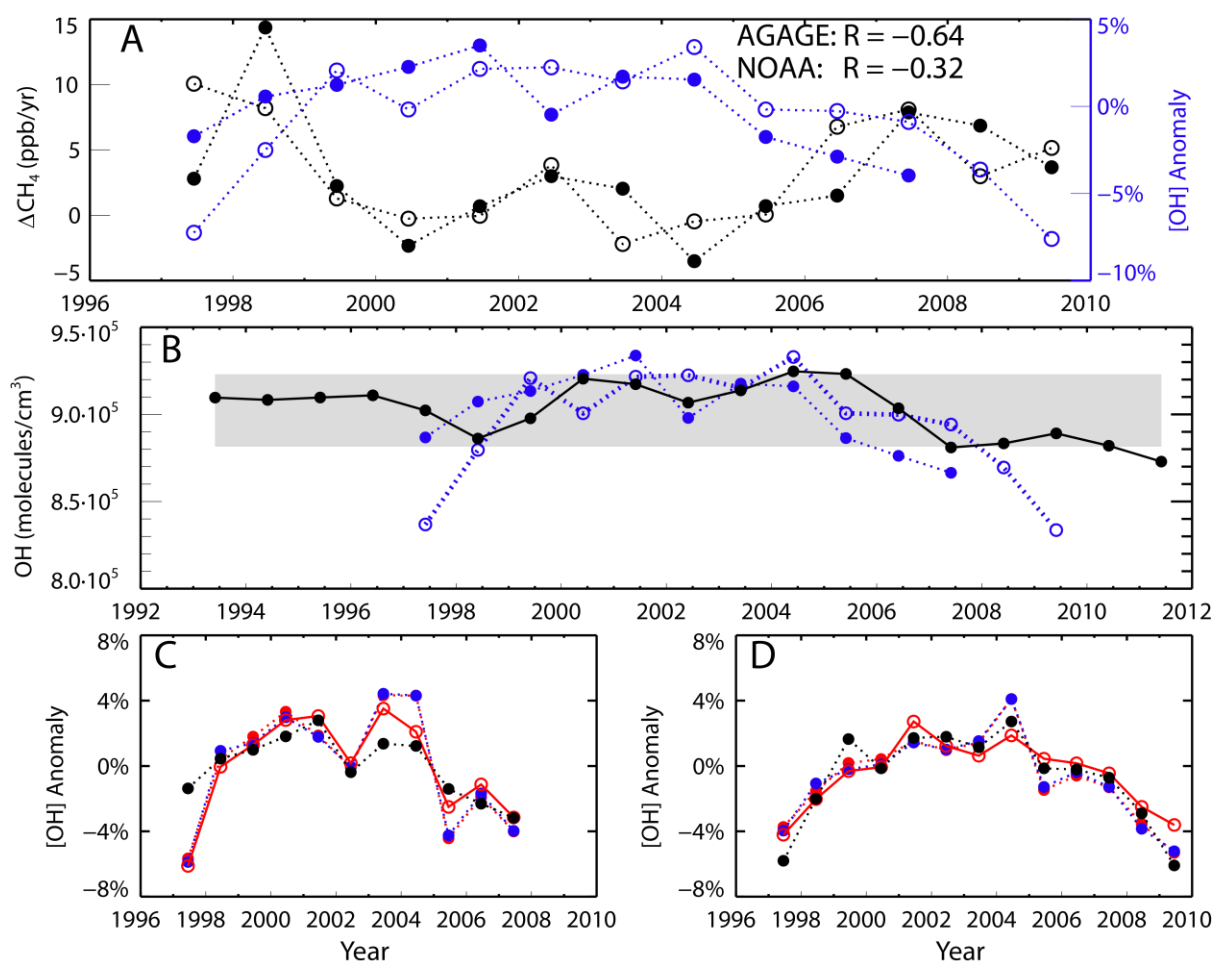
645 d. Fixed temperatures use zonal mean ERA-Interim temperatures averaged over 1993-2009.

646 **Table 3.** Calculated methane changes over different time periods from selected TOMCAT
 647 experiments and the NOAA and AGAGE observation networks.

Model run or observation network	Global mean ΔCH_4 in ppb (ppb/yr)			
	2009-1993	1998-1993	2006-1999	2009-2007
RE_FTFW	85.0 (5.0)	47.2 (7.9)	32.9 (4.1)	4.3 (1.4)
RE_FTVW	82.2 (4.8)	48.2 (8.0)	27.8 (3.5)	5.4 (1.8)
RE_VTVW	74.6 (4.4)	45.6 (7.6)	23.1 (2.9)	5.3 (1.8)
AP_FTVW ^a	97.7 ^e (5.7)	62.3 ^e (10.4)	8.2 ^g (1.0)	26.4 (8.8)
AL_FTVW ^b	104.2 ^e (6.1)	58.4 ^e (9.7)	17.3 (2.2)	27.5 (9.2)
NP_FTVW ^c	86.2 ^f (5.1)	49.7 ^f (8.3)	24.8 (3.1)	10.6 ^f (3.8)
NL_FTVW ^d	91.4 ^f (5.4)	58.8 ^f (9.8)	20.1 (2.5)	11.3 ^f (3.8)
NOAA obs.	56.1 (3.3)	36.0 (6.0)	4.8 (0.6)	14.7 (4.9)
AGAGE obs.	66.3 (3.9)	42.6 (7.1)	5.6 (0.7)	17.4 (5.8)

- 648
 649 a. Taken from Rigby et al. (2013) and Patra et al. (2011).
 650 b. Using 1997-2009 relative annual changes in mean [OH] derived from AGAGE data
 651 (Cunnold et al., 2002).
 652 c. Taken from Montzka et al. (2011) and Patra et al. (2011).
 653 d. Using 1997-2007 relative annual changes in mean [OH] derived from NOAA data (Prinn
 654 et al., 2015).
 655 e. Value using mean [OH] from 1993-1996.
 656 f. Value using mean [OH] from 1993-1996 and 2008-2011.
 657 g. Trend value not statistically significant at the 90% level.

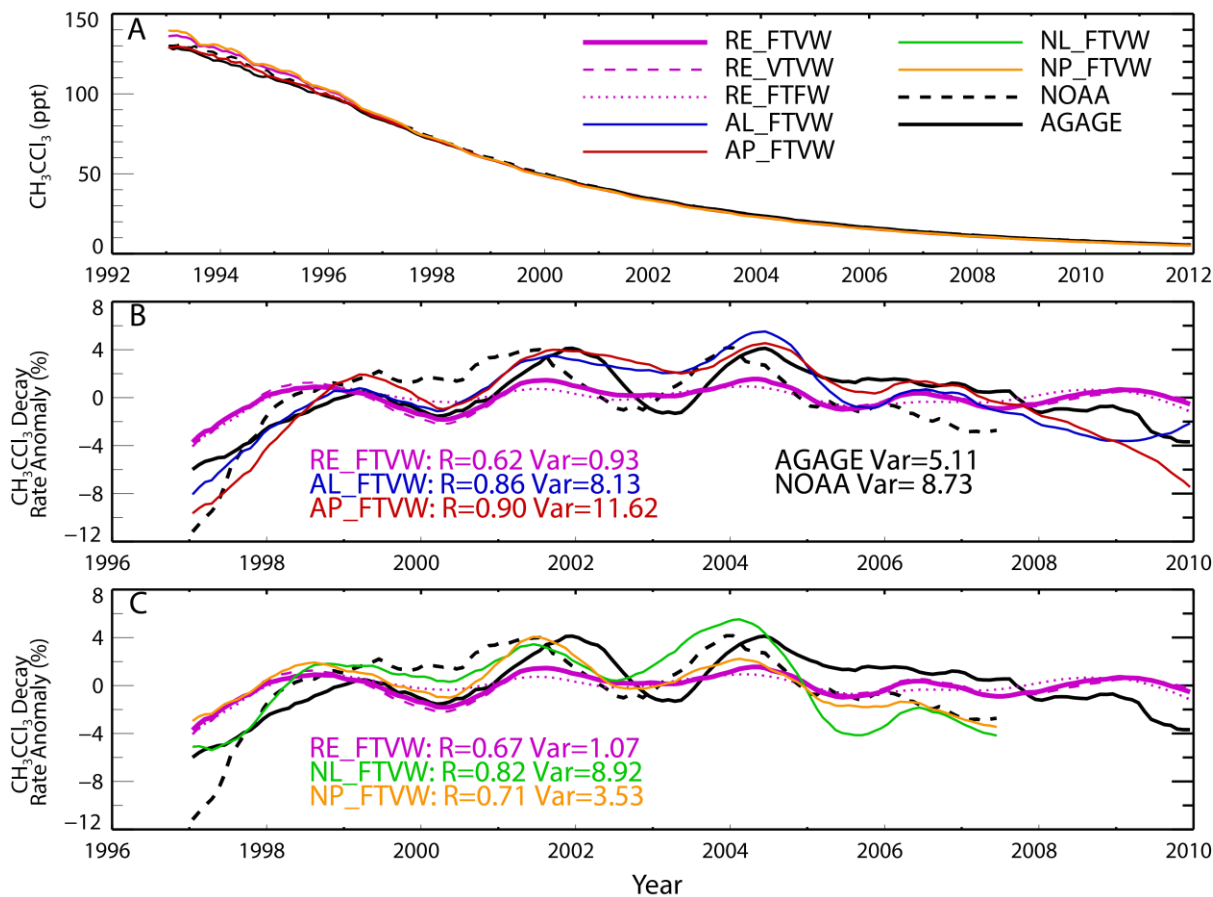
658 **Figures**



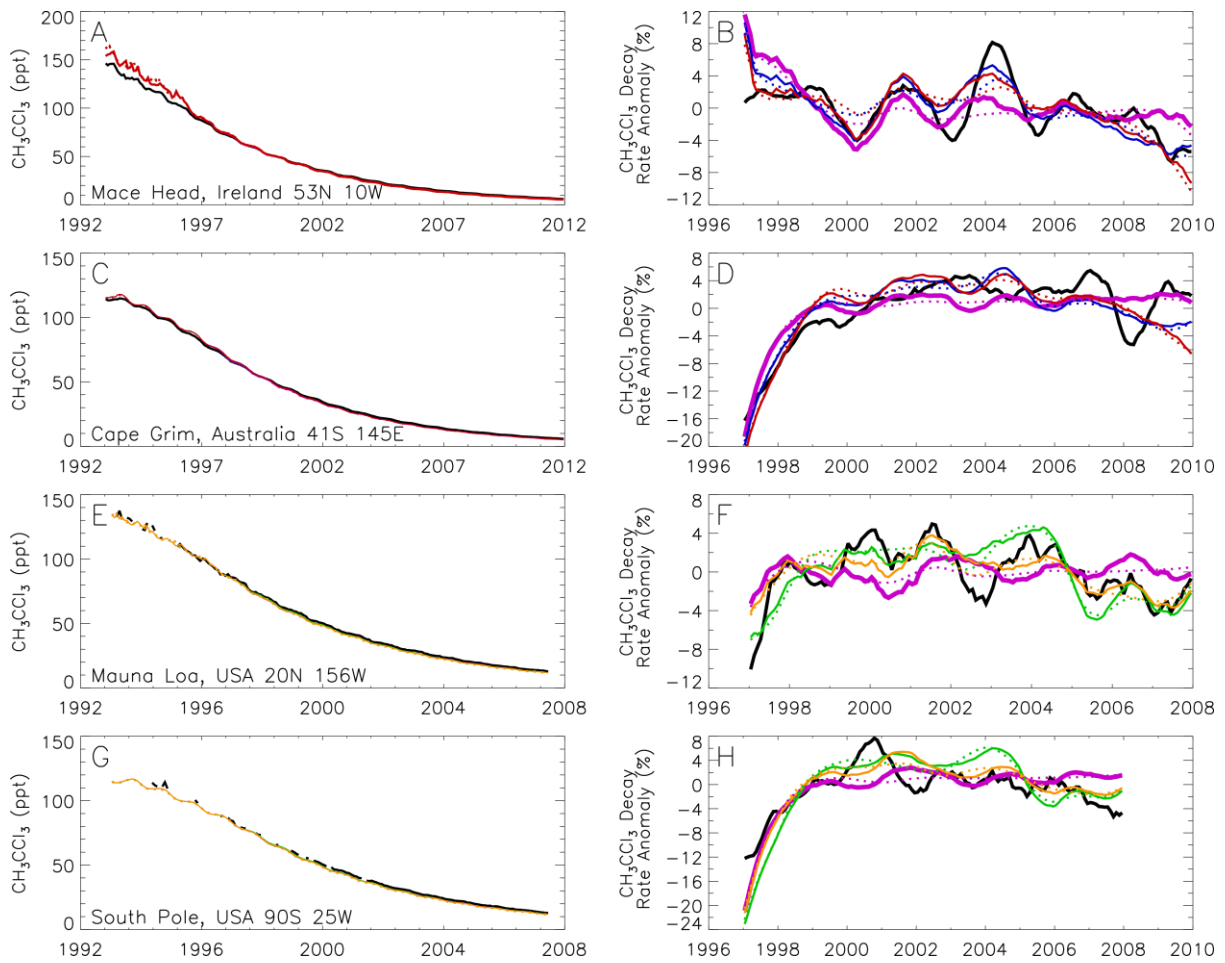
659

660 **Figure 1.** (a) Annual global CH_4 growth rate (ppb/yr) derived from NOAA (filled black circles)
 661 and AGAGE (open black circles) data (left hand y-axis), and published annual global [OH]
 662 anomalies derived from NOAA (filled blue circles, 1997-2007) and AGAGE (open blue
 663 circles, 1997-2009) CH_3CCl_3 measurements (right hand y-axis) (see text). (b) Annual mean
 664 [OH] (molecules/cm³) required for global box model (see Supplement S1) to fit yearly
 665 variations in NOAA CH_4 observations assuming constant emissions and temperature ($E=553$
 666 Tg/yr, $T=272.9$ K), based on Montzka et al. (2011) (solid black line). The shaded region
 667 denotes [OH] deviation of $\pm 2.3\%$ from the 1993-2011 mean. Also shown are the NOAA- and
 668 AGAGE-derived anomalies from panel (a) for an assumed mean OH (see Section 2.1). (c) Our
 669 estimates of [OH] derived from NOAA CH_3CCl_3 calculated using a global box model
 670 (Supplement S1) using repeating (blue) and varying (red) annual mean temperature and the
 671 CH_3CCl_3 emission scenario from UNEP (2015) (filled circles and dashed lines). Also shown
 672 for varying temperatures are results using the emissions of Montzka et al (2011) (red open
 673 circles and solid line) based on (Prinn et al. 2005) and the NOAA-derived values from panel
 674 (a) (black dashed line and circles). (d) As panel (c) but for OH derived from AGAGE CH_3CCl_3
 675 observations.

676

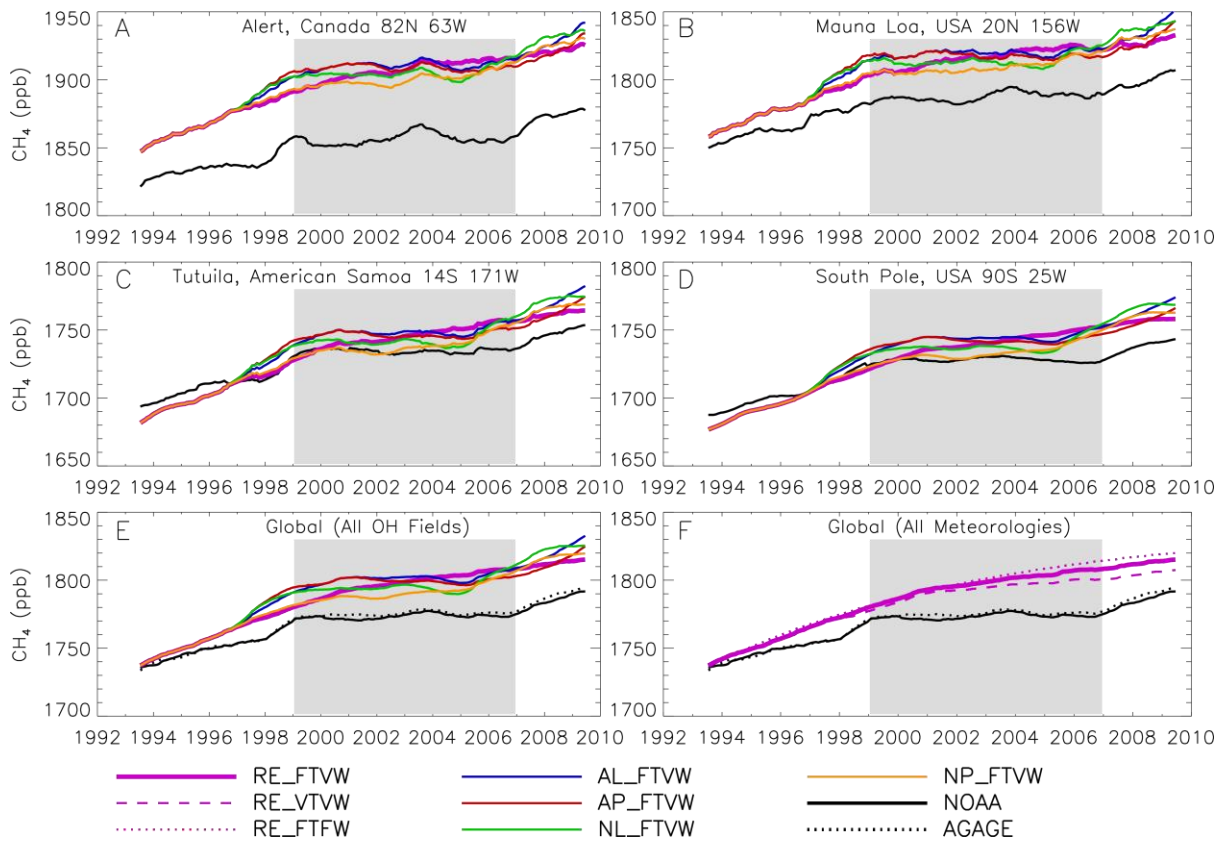


679 **Figure 2.** (a) Global mean surface CH_3CCl_3 (ppt) from NOAA (black dashed) and AGAGE
 680 (black solid) observations from 1993 to 2012. Also shown are results from five TOMCAT
 681 simulations with fixed temperatures and varying winds (see Table 1). (b) Global surface
 682 CH_3CCl_3 decay rate anomalies from NOAA and AGAGE along with model runs RE_FTVW,
 683 AL_FTVW and AP_FTVW (solid lines). Results from runs RE_FTVW and RE_VTVW are
 684 shown as a purple dotted line and dashed line, respectively. Observation and model anomalies
 685 are smoothed with a 12-month running average. Values given represent correlation coefficient
 686 when compared to AGAGE observations and variance. The decay rate anomaly is calculated
 687 from global mean CH_3CCl_3 values using equation (1) from Holmes et al., (2013), expressed as
 688 a percentage of the typical decay with a 12-month smoothing. (c) As panel (b) but for model
 689 runs NL_FTVW and NP_FTVW, along with RE_FTVW, RE_VTVW and RE_FTFW, and
 690 correlation coefficients for comparison with NOAA observations. The model results are split
 691 across panels (b) and (c) for clarity.



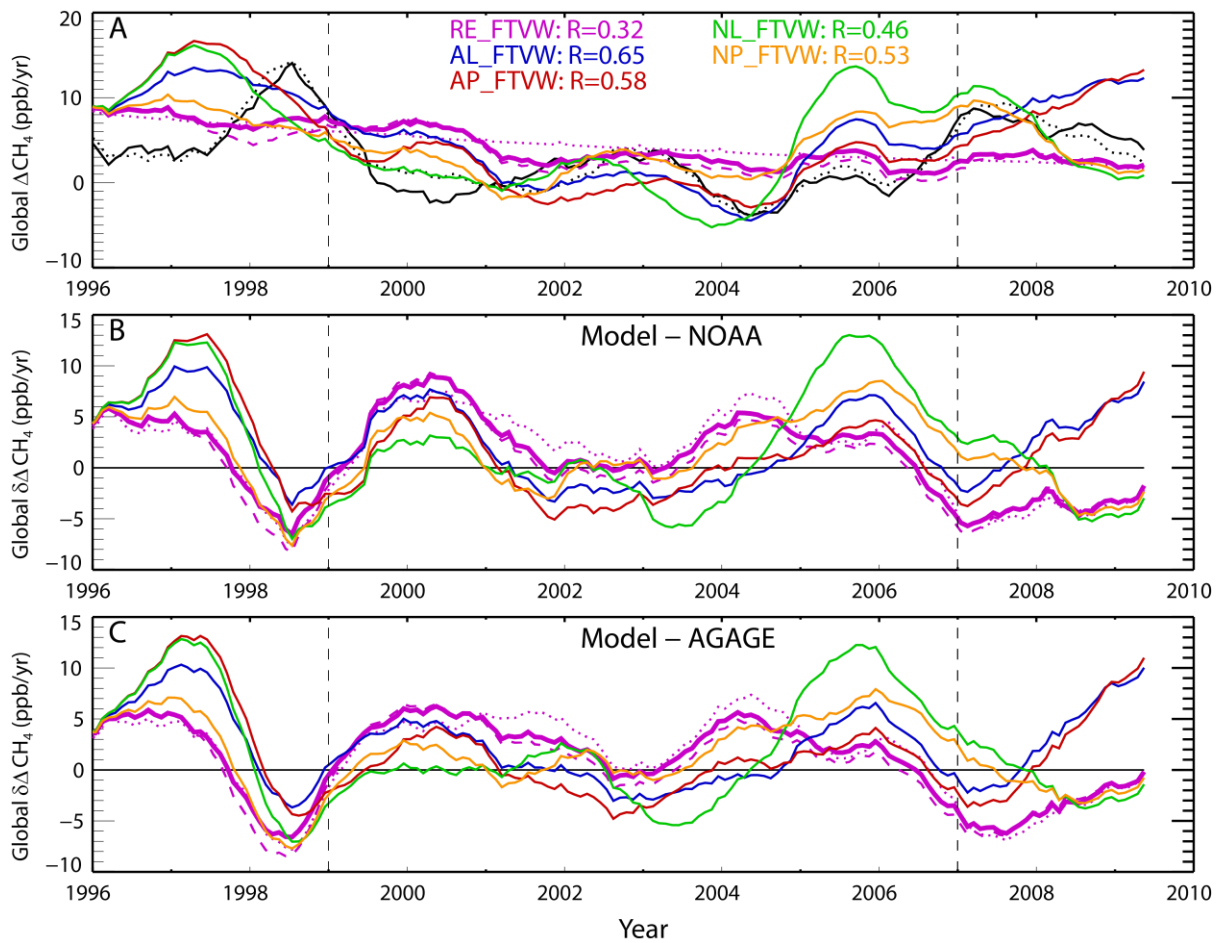
692

693 **Figure 3.** (Left) Observed mean surface CH_3CCl_3 (ppt) (black line) from (a) Mace Head
 694 (AGAGE), (c) Cape Grim (AGAGE), (e) Mauna Loa (NOAA) and (g) South Pole (NOAA).
 695 Also shown are results from five TOMCAT simulations with fixed temperatures and varying
 696 winds (FTVW, for legend see Figure 2a). (Right): Surface CH_3CCl_3 decay rate anomalies at
 697 the same station as the corresponding left column plot for observations (black), TOMCAT
 698 simulations with varying winds (FTVW, solid coloured lines) and TOMCAT simulations with
 699 fixed winds (FTFW, dotted lines). Comparisons at NOAA (AGAGE) stations show only
 700 comparisons with runs using NOAA (AGAGE)-derived OH, along with runs RE_FTVW and
 701 RE_FTFW in all panels.



702

703 **Figure 4.** (a, b, c and d) Deasonalised surface CH₄ (ppb) from 4 NOAA sites (black solid line)
 704 from 1993 to 2009. Also shown are results from five TOMCAT 3-D CTM simulations with
 705 fixed temperatures and varying winds (FTVW, see **Table 2**). (e) Deasonalised global mean
 706 surface CH₄ from NOAA (black solid) and AGAGE (black dashed) observations along with
 707 five TOMCAT simulations with different treatments of OH. (f) Same as (e) but for TOMCAT
 708 simulations using repeating OH (RE) and different treatments of winds and temperature. All
 709 panels use observation and model values which are smoothed with a 12-month running
 710 average. The shaded region marks the stagnation period in the observed CH₄ growth rate.



711

712 **Figure 5.** (a) The smoothed variation in the global annual CH₄ growth rate (ppb/yr) derived
 713 from NOAA (black solid) and AGAGE (black dashed) observations. Also shown are the
 714 smoothed growth rates from five TOMCAT 3-D CTM simulations with fixed temperatures and
 715 varying winds (FTVW, see Table 1). Values in legend give correlation coefficient between
 716 model run and NOAA observations. Also shown are results from runs RE_FTVW and
 717 RE_VTVW as a purple dotted line and dashed line, respectively (b) The difference in smoothed
 718 growth rate between TOMCAT simulations and NOAA observations shown in panel (a). (c)
 719 Same as (b) except using differences compared to AGAGE observations. The vertical dashed
 720 lines mark the start and end of the stagnation period in the observed CH₄ growth rate (1999 –
 721 2006).